Displacement monitoring of a Long-Span Arch Railway Bridge using Digital Image Correlation (DIC)

Ataei, S[1*], Shariatzadeh, M[2]

[1]Associate Professor, School of Railway Engineering, Iran University of Science and Technology, Tehran, Iran

[2]Ph.D. Student, School of Computer Science, Iran University of Technology, Tehran, Iran

ARTICLE INFO	A B S T R A C T
	Abstract There is an escalating demand for condition monitoring enhancement of transport infrastructures worldwide. Bridges are of vital importance in transportation infrastructure and need such monitoring. In this research, a non-contact vision-based technique called Digital Image Correlation (DIC) was used to calculate the bridge displacements. A high frame rate camera with 4K capability was used for raw data acquisition and simultaneous feature tracking. Also, a noise reduction filter is employed to make the measurements errors negligible. The displacement of the main span was calculated with an error of 0.08 pixel with 180 Frames Per Second (FPS) from a distance of about 200 meters. The obtained results by DIC were validated with those acquired from the verified FE model. It was concluded that the Digital Image Correlation method has acceptable proficiency and suitable precision for displacement measurement. Thus, it can be used as an alternative to traditional bridge displacement measurement instruments.

1. Introduction

The Bridge displacement measurements can be performed directly and indirectly. Direct methods include installation of traditional sensors through having physical contact with the bridge, which requires appropriate equipment for accessing the critical elements of the bridge. Also, wiring for power supply and data acquisition can be problematic. Recently, Liu et al. (2019) measured the displacement of a bridge in service by a hybrid reference-free sensing technology. First, a low-pass filter (LPF) was applied to accelerometer data to obtain the pseudostatic displacement, and then a high-pass filter was employed on the passive-servo electromagnetic-induction (PSEMI) data to acquire the dynamic displacement. Many studies have introduced new methods based on indirect bridge monitoring. There are various indirect techniques for displacement measurement, among which are inclinometers (Burdet & Zanella, 2000), and curvature measurement (Inaudi et al., 1998; Inaudi et al., 2002). Global Positioning System (GPS) (Wang et al., 2016; Casciati & Fuggini, 2011), laser vibrometer (Casciati & Wu, 2013) and interferometry system (Pieraccini et al., 2007) are among the other types of non-contact indirect methods which might be used in bridge displacement measurements.

The non-contact vision-based approach was also developed and applied by different

*Corresponding author
Email address: ataei@iust.ac.ir

researchers (Pan et al., 2016; Ribeiro et al., 2014; Choi et al., 2011; Lee & Shinozuka, 2006). Pieraccini (2013) published a systematic survey on the subject of ground-based radar interferometry (GBRI) and its practical cases. Recently, a bibliographic review of the related studies on GBRI was provided (Pieraccini & Miccinesi, 2019). Fukuda et al. (2013) have developed a robust object search algorithm for accurate tracking of feature points in the image without using any installed target on the structure. Jauregui et al. (2003), and Leitch (2002) conducted research based on digital close-range terrestrial photogrammetry contained laboratory and field tests. In addition to the displacement determination for the studied bridge, the authors can achieve the level of composite action by comparing the test results to which obtained from the finite element analysis. A new close-range photogrammetric bridge displacement measurement system was also developed by Jiang & Jauregui (2010) in which the work was verified through laboratory and field test. Olaszek (1999) applied a method based on the observation of particular spots of a bridge structure by taking advantage of CCD camera with telephoto lens to obtain the dynamic characteristics. A black cross on a white background selected as the pattern to be placed at the analysis points and an optical system by CCD matrix was used for imaging. Analysis of consecutive images provided information for displacement calculation of the observed points. Caetano et al. (2011) implemented a vibration monitoring test using a vision system contained a mounted camera with high-quality lenses. The researchers applied two methods for tracking the points: The Correlation and the optical Flow. Based on the mentioned facilities and methods, an experiment was employed on a cable footbridge to obtain cable vibrations. Yoneyama et al. (2007) carried out a research based on the application of digital image correlation technique within the accuracy of one pixel with zero gradients. The loading pattern was based on the truck passages. The authors founded wellagreed results with those obtained by displacement transducer for the studied bridge. Santos et al. (2012) applied a vision-based technique for a long suspension bridge. The authors made some remarks about this experiment; one of them was the applicability of this method when the bridge displacement occurs on a plane parallel to the sensor's video camera. Mehdi Mirzazadeh & Green (2017) used

DIC and fiber strain sensors to measure crack widths, displacements, and strains of Reinforced concrete beams. They studied the effect of temperature variation on the accuracy of the results. Vicente et al. (2018) used a laser and video-based displacement transducer (LVBDT) to capture static vertical displacements. The camera was located on the bridge to detect displacements at one point. Hong et al. (2018) used long-gauge fiber Bragg grating (FBG) sensors to measure strain responses for monitoring the dynamic deflection of beam-like structures. Alipour et al. (2019) studied the application of 2D-DIC for measuring bridge displacements. They proposed a method for measuring displacements without requiring to set up a camera on a fixed ground reference.

The bridge in this study stretches 448 m across a deep valley, so traditional measurement sensors cannot be used. Hence, DIC is deployed to measure the vertical displacement of the main span. This technique focuses on capturing videos from specific points on the structure in order to determine the precise displacement arising from train passages. The system was located at a distance of about 200 meters from the truss-arch bridge (Figure 1). The procedure is performed in two steps:

1) Raw data acquisition through recording the videos of the tests
2) Off-line data analysis and information extraction with high precision

The algorithm applied here tracks small square patches around the feature points from one frame to the other in a multi-resolution manner. This method also provides sub-pixel (0.08 pixel) accuracy in the tracking key points for displacement measurement. Then, calibration procedures and neutralization of perspective effects are performed. Finally, the results are validated by the verified 3D finite element model built by a commercial finite element software, SAP2000 (Wilson & Habibullah, 2017).

In addition to the DIC technique, which was described here, there are other suggested methods. One of the applied techniques is to use the calibrated stereo cameras (a pair of film recording cameras). Besides, a comparative study was made between photogrammetry and moiré photography (Forno et al., 1991). A good survey on several related studies can be found in the work of Jiang et al. (2008).

(a)

(b)

Figure 1. (a) Filming position, (b) Camera angle relative to the truss-arch bridge

Figure 2. The long-span steel-truss arch railway bridge

2. Material and Methods

2.1. Bridge properties

The studied railway bridge is located in Khoy County, Iran. It was completed and placed in service in 1970. One of its spans is a steel-truss arch with a length of over 223 meters. Including this span, the bridge is composed of 9 spans. Other spans are made of concrete piers or abutments. The bridge deck is made of steel. This long-span railway bridge has a total length of 448 m, and a height of 128 m from the base of the valley (Figure 2).

2.2. Loading condition

Based on a planned test, a predefined loading pattern was applied to the bridge. A test train composing of three locomotives (GT-26 type), six freight wagons, and one coBus was considered for loading. Freight wagons were filled with ballast. In order to model the load applied to the bridge, the distance between the axles was measured (Figure 3). The experiment was carried out using the test train running at different speeds, with the maximum allowable speed of 65 km/hr. The properties of the test train are tabulated in Table 1.

### 2.3. Specifications and arrangement of measuring equipment

The loading test was performed in static, dynamic, braking, and acceleration categories. Tests were carried out using a total of 32 sensors consisting of 3 Linear Variable Differential Transformers (LVDTs). Details of the tests and measurement equipment are available in a report by Ataei (2015). Since the bridge height was

Table 1. The properties of locomotives and freight wagons

Type of vehicle	Number of axles	Weight of full wagon (Ton)	The distance of two Bogies, center to center (m)	Distance between bogie axles (m)	Tampon to Tampon distance (m)
Locomotive (GT26)	6	110	12.50	2.03-1.70	21.10
Freight wagon	4	72	9.82	1.80	14.66

(a)
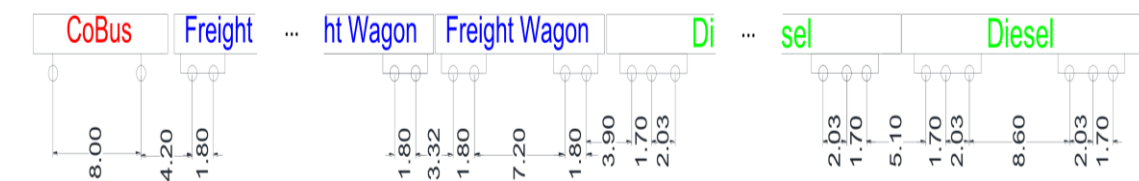
(b)

Figure 3. (a) Test train on the truss-arch bridge, (b) Distance between the axles of the test train (m)

more than 100 m, it was hard to perform dynamic measurements. Hence, the DIC technique is used for displacement measurements.

2.4. Configuration of the Vision-Based System

Installing traditional sensors for displacement measurement on a bridge of this nature is a very challenging task. Since the bridge height is more than a hundred meters, it was hard to perform dynamic measurement of the girder relative movements. Hence, several possible techniques were reviewed to find a suitable method for displacement determination. Consequently, the non-contact vision-based procedure was selected to be implemented using a 4K high frame rate camera (180 FPS).

Moreover, a telephoto lens was provided for the project. The camera was located on the nearest adjacent area to the bridge to capture the vertical displacement of the structure. In each step, by taking advantage of the telephoto lens, each feature point was tracked (Figure 4).

The recording was started before the arrival of the train to the specified section and during the train passage. The vertical displacement of the bridge girder was stored as a film to be analysis in a self-developed software, in order to extract the desired information of each frame in a specific time. In summary, all the accessories and recorded films used in this experiment have the following properties:

►Camera
■ Film recording was performed by SONY PXW-FS7 Camera.
■ Presetting was Slow and Quick Motion.
►Sensor Properties
■ The shutter of the camera was Global.
■ Noise amplitude in the picture was low and cannot be recognized visually.
■ The pictures were recorded with the quality of 1080x1920 (enjoying aspect ratio 16/9) and the frame rate of 179.82 FPS.
►Video Coding Properties
■ The digital format of video compression is **AVC100CBG_1920_1080_H422IP@L41** stored with the rate of 29.97 FPS
■ The size of each frame is 515 KB, and the real-time bit rate of the film is 93 MB per second (about 5.5 GB per minute).
►Environmental Conditions
■ The recording started at about 10 o'clock on a sunny morning and in the natural light condition.

The camera tripod has been fixed to the ground beneath.

2.5. Video Processing

The hardware mentioned above recorded the required films for data processing purpose. The films contain the period in which there were no loading on the bridge as well as the time of the train passage.

As the procedure is based on tracking key points among the frames, the first step is choosing the position of the feature points on the first frame. Then the positions should be updated from one frame to the next. The feature points that are tracked correctly among all frames and are near the desired area of the structure should be chosen from the last frame, which provides the information to be processed next. Two consequent analyses are the noise reduction and perspective correction that provide the appropriate final measurements.
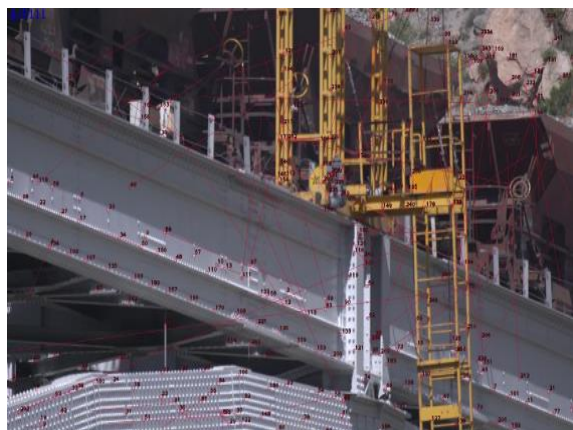

Figure 4. All feature points have been tracked for sub-pixel accuracy

2.6. Feature Point Detection

In this step, the recorded files are processed automatically. For the first frame, the feature points are selected based on the "Good Features to Track" algorithm for corner detection (Shi & Tomasi, 1994) which prefers the sharpest corners on the image while avoids choosing all the points from a small area by forcing the points to have a minimum distance (in this work fixed at 10 pixels). This issue ensures that there are enough feature points in any part of the image and avoids the absorption of all the feature points in a noisy background. At most 200 feature points were selected by the algorithm. The feature point detection was performed only on the first frame, followed by feature point

tracking in all consequent frames, as described next.

2.7. Feature Point tracking

An essential step in the video processing procedure is precisely tracking the selected corners from one frame to the next, to follow the coordinate's displacement of the key points. In practice, a small square patch around each point represents the feature point to make the tracking procedure possible and also robust to noise and degradation of the image sequence. A straightforward approach to track the patches is the correlation which uses searching the patch in a candidate area in the target frame around the original position and choosing the position with the least difference as the best match. However, this method is computationally expensive and also only provides integer precision. The wellknown Lucas-Kanade (LK) algorithm for feature point tracking (Pieraccini et al., 2007) solved both problems by taking advantage of a multiresolution pyramid from the original and target frames. The algorithm iteratively advances the best matching candidate position based on the spatial derivatives of the patch pixels in both horizontal and vertical directions. A vital property of the LK algorithm is its sub-pixel accuracy which estimates the actual movement of the physical position represented by the original patch precisely as if it was captured as a continuous 2D signal followed by a low-pass filter (LPF). In practice, it was determined that the patch sizes between 5x5 and 13x13 do not alter the results; hence, its size was fixed to 11x11. Note that the algorithm may result in totally incorrect outcomes whether the patch does not contain pixels with high derivatives (sharp edges) or the local pattern of the patch iterates nearby (which sometimes happens in the case of videos here). The noises from the original captured video or the compression algorithm also reduce the accuracy.

For all consequent frames, feature points are tracked with sub-pixel accuracy using DIC method. The output of this step is a film that consists of all feature points and numerical data of displacement for the points in each frame (Figure 5).

After obtaining results from the automated processing, the output film needs to be reviewed to determine which feature points are located on

the desired section, and also it is of vital importance that they are accurately tracked. By inspecting the last frame (with the visualized tracked points), several feature points that correctly tracked and located in the section of interest can be easily selected.

(a)

(b)

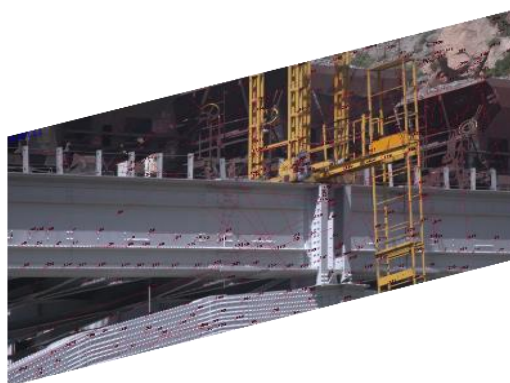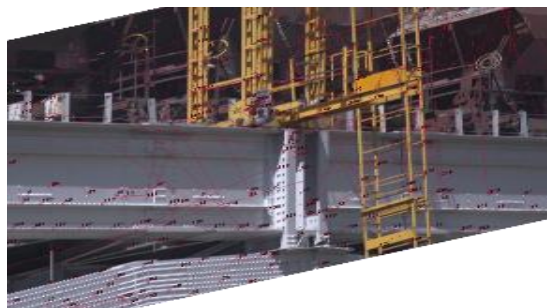Figure 5. (a) Feature detection, (b) Feature point tracking

2.8. Perspective Correction

The next step is the conversion of the scale from pixel to millimeter. It is known that when the focal length approaches infinity (as in our telephoto lens), the image formation would be close to "parallel projection" rather than perspective (Hartley & Zisserman, 2000) (Note that the parallel projection here is not orthographic). By applying a geometric affine transformation, it is possible to convert the image from its original state (side view) to a virtual one in which the vertical and horizontal scales are in millimeters. Figure 6 is the transformed version of Figure 4.
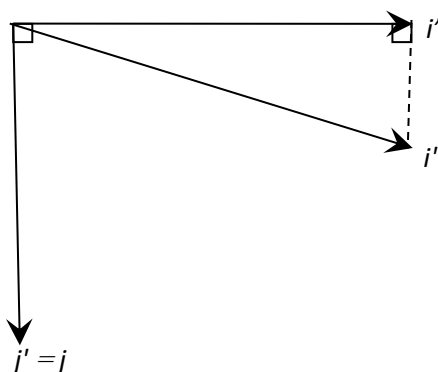

Figure 6. Applying an affine transform to the original image of the bridge girder in Figure 4

(a)

(b)

(C)

Figure 7. (a) Unit vectors of physical length on the bridge after applying the affine transform, (b) Inverse transform of unit vectors (7(a)) in the main image, (c) Procedure to project the vectors of 7(b) into horizontal and vertical axes of the image.

In order to apply an inverse transform to obtain a precise image of the bridge side view in perspective state, the coordinates of four points of the image are required. If there is an image with a parallel state, the coordinate information of three points is needed. However, in this case, it was possible to have even fewer data to fulfill the analysis. Since the vertical axis of the structure was along the vertical axis of the image with reasonable accuracy. For the other direction (horizontal direction), it applied with less precision. In the performed case, in order to compute the bridge displacement, it was not required to calculate a complete form of affine transform; therefore, obtaining a criterion would satisfy the conversion of the image length and width to millimeters.

In other words, if the horizontal and vertical unit vectors in Figure 7(a) are in millimeter; it would be enough to have equivalent vectors before any implementation of the affine transform (Figure 7(b)). According to the linear properties of vector operations, vector i" coefficients are converted into millimeters (Figure 7(c)).

In other words, the camera is positioned in a way that the vertical axis in the real world (e.g., the vertical axis of the bridge) coincided with the vertical axis of the picture. It is important to emphasize that two assumptions were made here. First, the focal length approaches infinity, and second, the points on the bridge have only two degrees of freedom. These assumptions are acceptable. The affine transform results in an acceptable metric and orthogonal image.

2.9. Noise Reduction

The final step consists of error reduction of feature points and derivation of required curves. The procedure is as follows:

Displacement data x and y for feature points derived from the processed video appear in a digital output file which contains two columns of data accompanied with time axis (t), are processed with a moving average filter with a window size of 20.

2.10. Pixel conversion to a Physical representation

The conversion of pixel to millimeter was performed by applying a simple coefficient.

Besides, a factor was applied to convert pixels to millimeters in the horizontal direction, which is equivalent to the vector i" in Figure 7(c) and was obtained from the horizontal distance of two points on the bridge (without considering the vertical distance of the points). Horizontal displacements in millimeters can also be computed by taking advantage of this factor.

After determining the transformation coefficients in both vertical and horizontal directions, all the required information related to the feature point position are obtained. In this step, the time-displacement curve of the feature point has been used to obtain the required time period of the no-loading condition and the test duration. As the location of a feature point in the no-load time period is considered as coordinate origin, the average point displacement in this period would be computed as zero shift. Moreover, the standard deviation of feature point displacement could also be calculated and considered as the experiment error.

2.11. Error Analysis and Reduction

The lack of error analysis and reduction can be observed in previous studies. Hence, in the current study, the evaluation of error factors in the measurement procedure is performed. The sources of error or its reduction are categorized as follows:

1) Imaging (includes camera sensor noise, the vibration of a camera tripod, and lens distortion)
2) Initial data extraction from the recorded film (error of inaccurate tracking of feature points, the estimation error of parallel modeling for the camera, errors in coefficients used for conversion of pixel to physical length unit for both horizontal and vertical directions)
3) Employing filters that incorporate Digital Signal Processing (DSP) and data processing procedures (denoising via data combination and filtering)

If the location of the ith feature point in the frame t is considered, it can be shown by P_i (t), as follows:

$$P_i(t) = \big(x_i(t), y_i(t)\big), \qquad i = 1..n \qquad (1)$$

For error estimation, it is possible to use displacement error of feature points in noloading

condition. In other words, in no-loading condition, it is expected not to observe any displacement of feature points; otherwise, it is considered as noise. For this aim, it is assumed that a unitary feature point with I index is used. The no-loading period was called t0...t1. As the vertical displacement is significant, the standard deviation index of error was computed for the vertical direction. Consequently, the standard deviation of error is defined as:

$$e_s = std(y_I(t))_{t=t_0...t_1} \qquad (2)$$

The index above was applied for evaluation of processing error. The value of e_s in current experiments was about 0.24 (0.08 pixel). In other words, with the assumption of a normal distribution for error, the 95% confidence interval was about 0.5 pixels. It indicated the role of the first two steps in raw error creation. By considering a transformation coefficient of 5 millimeters per pixel, the raw error of measurement and displacement recording (with 95% confidence interval) would be about ±2.5 millimeter.

To improve the results, two methods of data combination were applied. One is based on increasing the number of points in each frame (Spatial), and the other is according to filter implementation in the time dimension (Temporal). The average displacement of 4 feature points was considered as the new feature point in the first case, which means:

$$y_I = \overline{(y_i, y_j, y_k, y_l)} \qquad (3)$$

Also, in the second case, the displacement function in the time period is convolved with a kernel of low pass filter. In other words,

$$y'_I(t) = y_I(t) * K(t) \qquad (4)$$

In which K(t) is a uniform kernel with the length of 20 frames (about 0.11 s). By applying larger windows, the results did not change.

In the first method of denoising, the difference between the error standard deviation of a point, and the one for 4 points was not substantial. As can be seen from Figure 8(a), the points selected on one pier, practically have similar errors. Hence, the error factors in feature points tracking are not independent. For instance, errors of the feature point tracking algorithm or camera sensor noise, which are

independent for various points on the image, have negligible effects.

In contrast, dependent errors like shaking of a camera tripod, which affects all tracking points simultaneously, are considerable in the recording procedure. For that reason, all three lines are highly similar (Figure 8(a)). In this experiment, the value of the standard deviation of displacement for each of the 4 points varied from 0.2 to 0.25 pixel; while the mean value of all four points had a standard deviation value of 0.24 pixels.

When using a uniform kernel, the standard deviation reaches 0.08 pixels. The lines which are near the coordinate origin can prove this statement (Figure 8(b)). In the case of not using LPF, the error of feature points forms a halo from adjacent points. While in the output of LPF, this spot is much smaller and more condensed; because in the no-loading condition, the points do not move that much. In terms of the physical length unit, 95% confidence interval in this test is about ±0.75 millimeters, which is an acceptable accuracy.
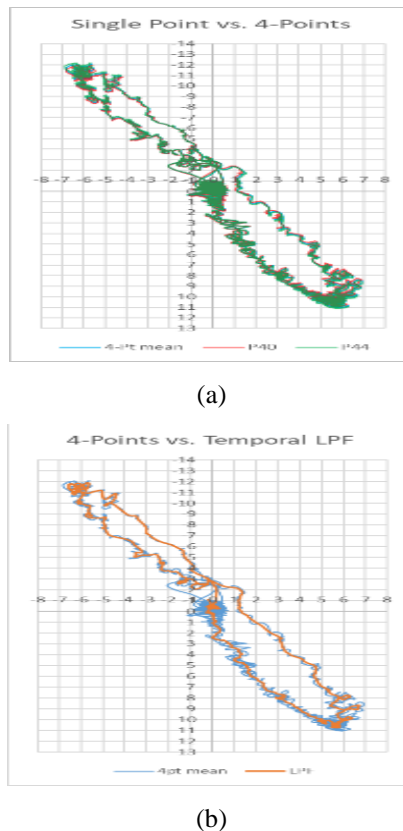

(a)

(b)

Figure 8. Displacement profile of feature point and error reduction methods, (a) Experiment by using 4-point averaging, (b) Low-Pass Filter in the time direction

Ataei et al.

2.12. Measured Displacement of the Bridge

The process discussed in the previous section was applied for capturing image sequences. The image processing procedure was performed by a self-developed software written in C++ using the OpenCV library (2015). Further analysis and visualizations were performed using Microsoft Excel and Matlab. Under all conditions, a point tracked precisely (during the film recording) on a specific part of the bridge is considered as the feature point. Figure 9 shows a view of the midspan, first and second section (Figure 10).

(a)

(b)

(c)
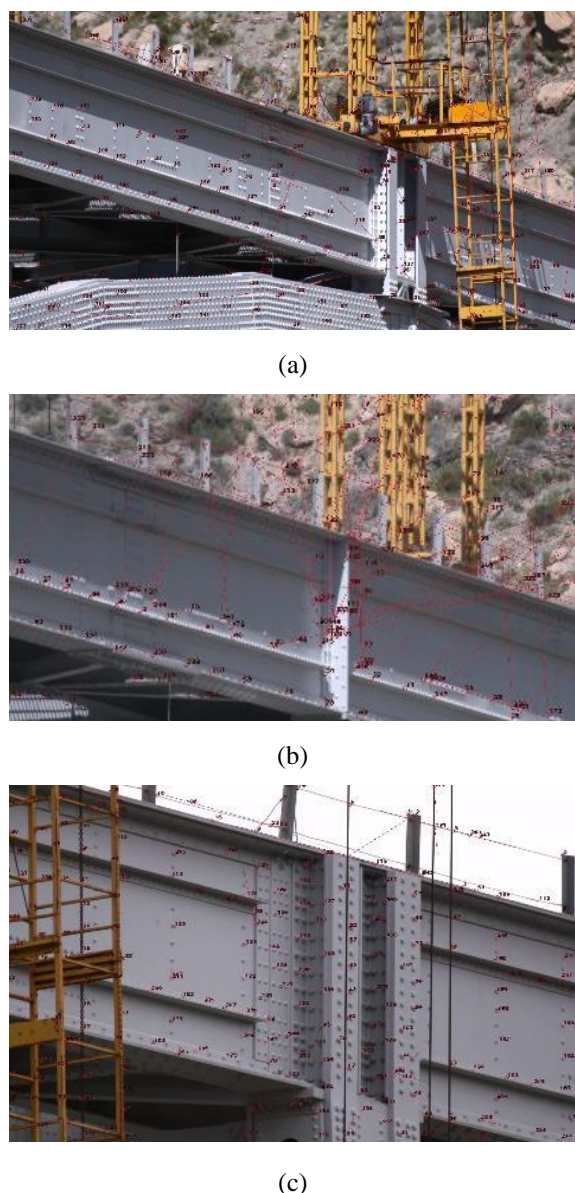
Figure 9. The physical position of the points in the image, (a) Midspan, (b) First section, (c) Second section

3. Discussion and Results

Tests locations and the measurement sections along the truss-arch bridge are illustrated in Figure 10. Based on the results mentioned in Ataei (2015), the impact factor of these tests are considered to be 1.0.

3.1. Measured Displacement of the Bridge

Sap2000, a commercial software based on finite element analysis, is used to model the bridge. Frame elements are used to model the structure (Figure 11). Bridge bearings are defined as pot bearings and are modeled using link elements. Also, the connection of longitudinal beams and the main arch is provided using pinned-link elements. The module of elasticity of steel was considered 200 GPa.

To create the FE model considering the current state of this truss-arch railway bridge, extensive in-situ measurements were performed by Ataei (2015). Frequency values obtained by field test and FE model are shown in Table 2.

The response of the validated model is compared to the measurements obtained through DIC. The results obtained using this model, conferme that it reproduces the dynamic displacement and force patterns observed by performing field test. The test train is composed of three six-axle diesel and six full wagons of ballast. The passing train was modeled as a moving force. Displacements acquired through DIC and analytical model are compared in Figure 12.

It can be seen that the first vertical frequency of the bridge is acquired by taking a fast Fourier transform (FFT) of the midspan displacement obtained by DIC (Figure 13).
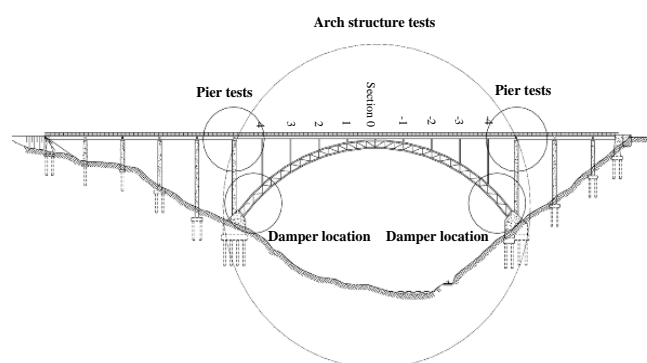

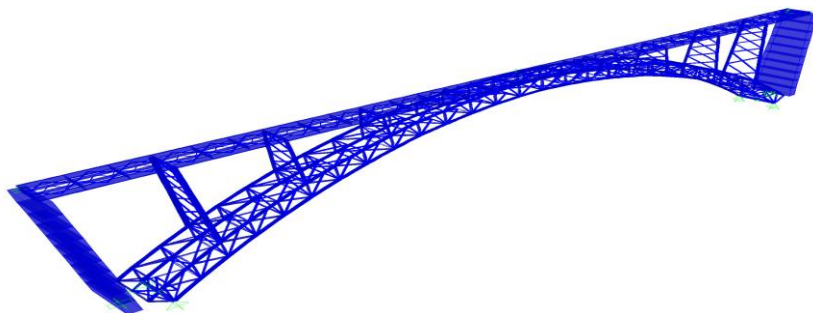Figure 10. Bridge sections and range of experiments

Figure 11. 3D finite element model of the truss-arch bridge

Table 2. Frequency values obtained through field test and numerical simulation (Ataei (2015))

| Mode Number	1	2	3	4	5
Mode Type	Transverse	Longitudinal	Transverse	Vertical	Transverse
Frequency (field test)	0.64	0.64	1.29	1.83	2.25
Frequency (FE model)	0.68	0.74	1.43	1.80	2.12

(a)
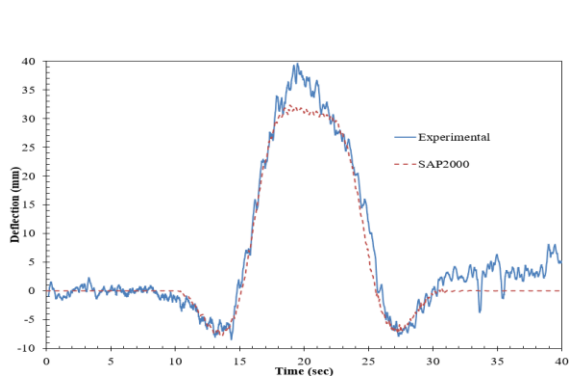
(a)
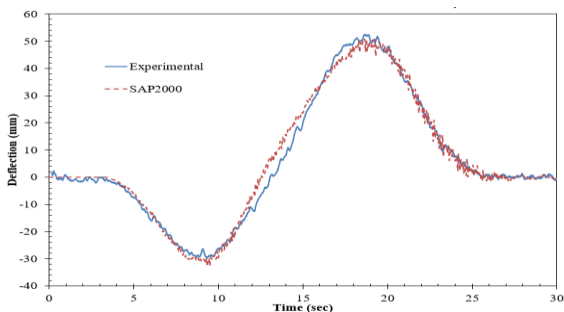
(b)

Figure 12. 3D Comparison of the displacements obtained from DIC and analytical model (a) Displacement of Mid span (Train Passage Direction: Left to Right-Speed 60 Km/h) (b) Displacement of Section 1(Train Passage Direction: Right to Left-Speed 55 Km/h)
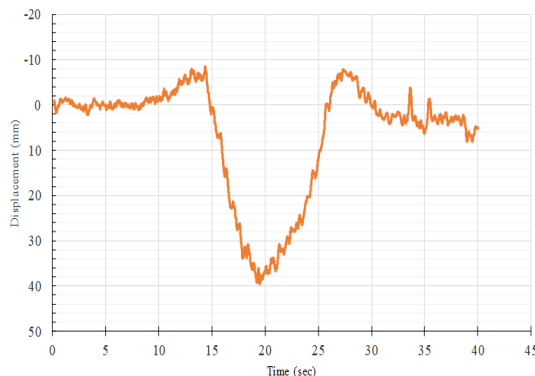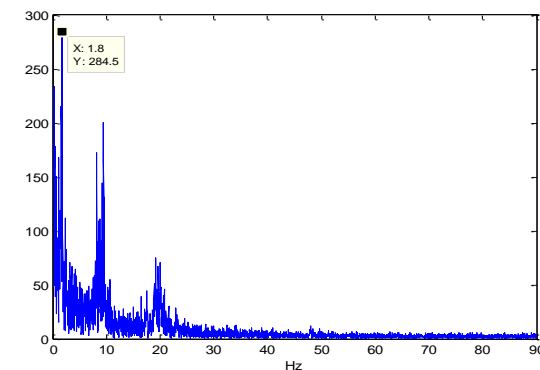
(b)

Figure 13. (a) Midspan displacement acquired through DIC (Train Passage Correction: Left to Right-Speed 65 Km/h), (b) FFT of the obtained midspan displacement data using DIC

4. Conclusion

In this research, the displacement of a longspan steel-truss arch bridge was measured. Due to its height, which is about 130 m, traditional methods of displacement measurements are very difficult to implement. On the other hand, the maintenance and response extraction of this bridge due to its vital importance in the railway network is inevitable. Consequently, the DIC technique has been used to measure the deck displacement from a distance of about 200 meters with 180 FPS and the error of 0.08 pixel. The results were compared to those obtained from the finite element analysis. According to the results, the error estimation and reduction method have acceptable proficiency and suitable precision (0.24 millimeter) for displacement measurement.

The following points are noticeable:

- Poor performance of humans does not have any effects on the accuracy of this method; the DIC technique is fast and precise.
- To measure the accuracy and validity of the tests, the error values of the static system has been considered as an unbiased criterion. The error of the system in each test could be assessed based on the defined criterion (because of unacceptable error level, one of the tests has been removed). Therefore, it is a way to verify the precision of each measurement.
- One of the advantages of DIC is to estimate the trend of errors accurately. Besides, error reduction could be observed after denoising.
- Simultaneous measurement of multiple points is very cost effective.

Acknowledgements

References

[1] Liu, B., Ozdagli, A. I., Moreu, F., & Chi, Q. (2019). "Hybrid reference-free total displacement for railroad bridge campaign monitoring". Measurement Science and Technology.

[2] Burdet, O., & Zanella, J. L. (2000, January). "Automatic monitoring of bridges using electronic inclinometers". In IABSE Congress Report (Vol. 16, No. 6, pp. 1574-1581). International Association for Bridge and Structural Engineering.

[3] Inaudi, D., Vurpillot, S., Casanova, N., & Kronenberg, P. (1998). "Structural monitoring by curvature analysis using interferometric fiber optic sensors". Smart Materials and Structures, 7(2), 199.

[4] Inaudi, D., Ruefenacht, A., Von Arx, B., Noher, H. P., Vurpillot, S., & Glisic, B. (2002, June). "Monitoring of a concrete arch bridge during construction". In Smart Structures and Materials 2002: Smart Systems for Bridges, Structures, and Highways (Vol. 4696, pp. 146-154). International Society for Optics and Photonics.

[5] Wang, J., Meng, X., Qin, C., & Yi, J. (2016). "Vibration frequencies extraction of the forth road bridge using high sampling GPS data". Shock and Vibration, 2016.

[6] Casciati, F., & Fuggini, C. (2011). "Monitoring a steel building using GPS sensors". Smart Structures and Systems, 7(5), 349-363.

[7] Casciati, F., & Wu, L. (2013). "Local positioning accuracy of laser sensors for structural health monitoring". Structural Control and Health Monitoring, 20(5), 728-739.

[8] Pieraccini, M., Parrini, F., Fratini, M., Atzeni, C., Spinelli, P., & Micheloni, M. (2007). "Static and dynamic testing of bridges through microwave interferometry". NDT & E International, 40(3), 208-214.

[9] Pan, B., Tian, L., & Song, X. (2016). "Real-time, non-contact and targetless measurement of vertical displacement of bridges using off-axis digital image correlation". NDT & E International, 79, 73-80.

[10] Ribeiro, D., Calçada, R., Ferreira, J., & Martins, T. (2014). "Non-contact measurement of the dynamic displacement of railway bridges

using an advanced video-based system". Engineering Structures, 75, 164-180.

[11] Choi, H. S., Cheung, J. H., Kim, S. H., & Ahn, J. H. (2011). "Structural dynamic displacement vision system using digital image processing". NDT & E International, 44(7), 597-608.

[12] Lee, J. J., & Shinozuka, M. (2006). "A vision-based system for remote sensing of bridge displacement". NDT & E International, 39(5), 425-431.

[13] Pieraccini, M. (2013). "Monitoring of civil infrastructures by interferometric radar: A review". The Scientific World Journal, 2013.

[14] Pieraccini, M., & Miccinesi, L. (2019). "Ground-Based Radar Interferometry: A Bibliographic Review". Remote Sensing, 11(9), 1029.

[15] Fukuda, Y., Feng, M. Q., Narita, Y., Kaneko, S. I., & Tanaka, T. (2013). "Vision-based displacement sensor for monitoring dynamic response using robust object search algorithm". IEEE Sensors Journal, 13(12), 4725-4732.

[16] Jáuregui, D. V., White, K. R., Woodward, C. B., & Leitch, K. R. (2003). "Noncontact photogrammetric measurement of vertical bridge displacement". Journal of Bridge Engineering, 8(4), 212-222.

[17] Leitch, K. R. (2002). "Close-range Photogrammetric Measurement of Bridge Deformations". PhD thesis, New Mexico State Univ., Las Cruces, N.M.

[18] Jiang, R., & Jauregui, D. V. (2010). "Development of a digital close-range photogrammetric bridge displacement measurement system". Measurement, 43(10), 1431-1438.

[19] Olaszek, P. (1999). "Investigation of the dynamic characteristic of bridge structures using a computer vision method". Measurement, 25(3), 227-236.

[20] Caetano, E., Silva, S., & Bateira, J. (2011). "A vision system for vibration monitoring of civil engineering structures". Experimental Techniques, 35(4), 74-82.

[21] Yoneyama, S., Kitagawa, A., Iwata, S., Tani, K., & Kikuta, H. (2007). "Bridge displacement measurement using digital image correlation". Exp Tech 311:34–40.

[22] Santos, C. A., Costa, C. O., & Batista, J. P. (2012). "Long deck suspension bridge monitoring: the vision system calibration problem". Strain, 48(2), 108-123.

[23] Mehdi Mirzazadeh, M., & Green, M. F. (2017). "Fiber Optic Sensors and Digital Image Correlation for Measuring Deformations in Reinforced Concrete Beams". Journal of Bridge Engineering, 23(3), 04017144.

[24] Vicente, M., Gonzalez, D., Minguez, J., & Schumacher, T. (2018). "A novel laser and video-based displacement transducer to monitor bridge displacements". Sensors, 18(4), 970.

[25] Hong, W., Qin, Z., Lv, K., & Fang, X. (2018). An Indirect Method for Monitoring Dynamic Deflection of Beam-Like Structures Based on Strain Responses. Applied Sciences, 8(5), 811.

[26] Alipour, M., Washlesky, S. J., & Harris, D. K. (2019). "Field Deployment and Laboratory Evaluation of 2D Digital Image Correlation for Displacement Sensing in Complex Environments". Journal of Bridge Engineering, 24(4), 04019010.

[27] Wilson, E. L., & Habibullah, A. (2017). "SAP 2000 software, version 19". Computer and Structures, Inc. (CSI), Berkeley.

[28] Forno, C., Brown, S., Hunt, R. A., Kearney, A. M., & Oldfield, S. (1991). "The measurement of deformation of a bridge by Moirè photography and photogrammetry". Strain, 27(3), 83-87.

[29] Jiang, R., Jáuregui, D. V., & White, K. R. (2008). "Close-range photogrammetry applications in bridge measurement: literature review". Measurement, 41(8), 823-834.

[30] Ataei, S. (2015). "Condition Monitoring of the Ghotour Bridge". Report submitted to the Iranian Railway Organization.

[31] Shi, J., & Tomasi, C. (1994). "Good features to track IEEE Conf. on Computer Vision and Pattern Recognition" (CVPR94) (Seattle).

[32] Hartley, R., & Zisserman, A. (2000). "Multiple view geometry in computer vision second edition". Cambridge University Press.

[33] OpenSource Computer Vision Library (OpenCV). (2015). Retrieved from www.opencv.org.